Applied Catalysis B: Environmental 180 (2016) 408–415

Contents lists available at ScienceDirect

Applied Catalysis B: Environmental

journal homepage: www.elsevier.com/locate/apcatb

Hydrogenation of nitrophenols catalyzed by carbon black-supported nickel nanoparticles under mild conditions

Jiawei Xia [a,b], Guangyu He [b], Lili Zhang [c,*], Xiaoqiang Sun [b,*], Xin Wang [a,*]

[a] Key Laboratory of Soft Chemistry and Functional Materials, Nanjing University of Science and Technology, Ministry of Education, Nanjing 210094, China
[b] Key Laboratory of Fine Petrochemical Engineering, Changzhou University, Changzhou 213164, China
[c] Jiangsu Key Laboratory for Chemistry of Low-Dimensional Materials, Huaiyin Normal University, Huai'an, Jiangsu 223300, China

ARTICLE INFO

Article history:
Received 2 February 2015
Received in revised form 23 June 2015
Accepted 24 June 2015
Available online 30 June 2015

Keywords:
Nickel nanoparticles
Carbon black
Catalytic hydrogenation
Nitrophenols reduction
Lower temperatures

ABSTRACT

A carbon black (CB) supported nano-Ni catalyst is prepared by a facile method using nickel chloride as the nickel source and hydrazine hydrate as the reducing agent. TEM observation shows that Ni nanoparticles have a good dispersion with a narrow size distribution on the surface of carbon black. The catalyst exhibits significantly high catalytic activity for hydrogenation of nitrophenols even at 30 °C. The high performance obtained here can be attributed to the specific characteristics of the nanostructure of the catalyst and the synergistic effect of nano-Ni and carbon black, including plenty of oxygen-containing groups of carbon black for anchoring Ni atoms, strong adsorption ability for organic molecules and good conductivity for electron transfer from the carbon black to Ni nanoparticles. Moreover, the Ni-based catalyst is relatively cheap and magnetically separable, thus achieving a low-cost hydrogenation of nitrophenols to aminophenols.

1. Introduction

Nitroaromatic compounds are being widely used in industrial processes, including the manufacture of dyes, pharmaceuticals, pigments, pesticides, wood preservatives and rubber chemicals [1–4]. Therefore, nitroaromatic compounds are often presented as water pollutants due to the release in industrial effluents. These pollutants pose significant health risks due to their carcinogenicity and may leave residues in animal products such as meat and eggs. Among various nitroaromatic compounds, nitrophenols are listed as one of top 114 organic pollutants by the United State Environmental Protection Agency (USEPA) [5,6], and especially, they have been implicated in carcinogenesis, teratogenesis and mutagenesis [5–7]. On the other hand, it is hardly inevitable that nitrophenols are a kind of important byproducts for the synthesis of nitro compounds, such as nitrobenzene, which can be produced through benzene nitration in the presence of mixed acid. Moreover, apart from mono-nitrophenols, di- and tri-nitrophenols (DNP and TNP) with stronger toxicity, carcinogenicity, mutagenicity and teratogenicity, are also significant byproducts in industrial processes [5,8,9]. Besides, the nitrophenols can also be produced in the air through the atmospheric photochemical reactions of nitrobenzene, bromobenzene and aromatic hydrocarbons with hydroxyl radicals and nitrogen oxides [10]. It is known that the reduction products of nitrophenols, aminophenols with lower toxicity are widely used as intermediates for the synthesis of pesticides, medicine, dyes and other fine chemicals [11,12]. As a typical example, *p*-aminophenol (*p*-AP) is less poisonous than *p*-nitrophenol (*p*-NP), and has become an important intermediate for the production of analgesic and antipyretic drugs such as phenacetin, paracetamol and acetanilide [3,13,14]. Therefore, for the sake of industrial mass production and the construction of environment-friendly society, it is of great significance to implement cost-effective strategy for the reduction of nitrophenols to aminophenols.

Several approaches for the reduction of nitrophenols to aminophenols have been reported so far, such as iron-acid reduction [1,2,15], electrolytic reduction [16], catalytic hydrogenation [17–21], etc. Iron-acid reduction requires strong acidic medium with low selectivity in general. In the meantime, a large amount of metal oxides is produced during the process, resulting in environmental problems. The electrolytic reduction is usually carried out in acidic or alkaline media and requires high energy consumption. Among all practicable routes mentioned above, only catalytic hydrogenation is a cost-effective process because this route can achieve high conversion efficiency with low emission under mild reaction conditions [22–24].

* Corresponding authors.
E-mail addresses: zll@hytc.edu.cn (L. Zhang), xqsun@cczu.edu.cn (X. Sun), wangx@njust.edu.cn (X. Wang).

http://dx.doi.org/10.1016/j.apcatb.2015.06.043
0926-3373/

Undoubtedly, the precious metal-based catalysts are still remain the leading catalysts for hydrogenation such as palladium [25–27], platinum [28–30], rhodium [31,32], ruthenium [33,34] and aurum-based [35–37] systems, even though their widespread applications are limited by their low earth-abundance and high cost. In order to solve these problems, various non-precious metal catalysts [38–40], especially nickel-based catalysts [3,39–41] have been developed as economical alternatives in hydrogenation reactions. However, compared with precious metal-based catalysts, the nickel-based systems usually exhibit relatively low activity, require higher temperatures and consume more energy in the process. Up to now, much less attention has been paid to the reduction of nitrophenols to aminophenols with nickel-based catalysts at lower temperatures [16,19].

Carbon black (CB), such as Vulcan XC-72, is one of the most commonly used supports for metal-based catalysts in many studies and commercial applications due to its turbostratic structures with high surface area and conductivity, especially, its lower cost when compared with nanocarbons [37,42]. Nevertheless, Vulcan XC-72 also suffers from the disadvantages such as its relatively lower content of oxygen-containing groups for anchoring precursor metal ions or metal nanoparticles and deep micropores or recesses which trap the metal nanoparticles making them difficultly accessible to reactants. It is known that the performance of XC-72 supported catalysts can be enhanced through modification, for instance, using acidification of XC-72 to produce more oxygen-containing groups.

Hence, it is of great interest to develop a carbon black supported nano-Ni catalyst for the hydrogenation reactions of nitrophenols under mild conditions. If that can be accomplished, then it may be possible to achieve the cost-effective hydrogenation of nitrophenols to aminophenols. Herein, we report a facile strategy for the preparation of Ni/CB system as an advanced catalyst for hydrogenation of nitrophenols to aminophenols. It is found that the Ni nanoparticles (Ni NPs) are well dispersed on the surface of carbon black and have a narrow size distribution. The Ni/CB catalyst exhibits significantly high catalytic activity for hydrogenation of nitrophenols at lower temperatures, thus its performance is impressively higher than that of recently reported nickel-based nanocatalysts [1,2,18]. Compared with noble metal-based catalysts, this catalyst is much cheaper and magnetically separable. Such a catalyst facilitates achieving the cost-effective hydrogenation of nitrophenols to aminophenols.

2. Experimental

2.1. Materials

Ethylene glycol (EG, 99.0%), nitric acid (HNO_3, 65–68%), hydrazine hydrate ($N_2H_4{\cdot}H_2O$, 50%), nickel chloride ($NiCl_2{\cdot}6H_2O$, 98%), *o*-nitrophenol (*o*-NP, 98%), *m*-nitrophenol (*m*-NP, 99%) and *p*-nitrophenol (*p*-NP, 99.0%) were all of analytical grade and supplied by Sinopharm Chemical Reagent Co., Ltd. Sodium borohydride ($NaBH_4$, 98%), sodium hydroxide (NaOH, BP. 98–100.5%) were obtained from Aladdin Industrial Cooperation. Vulcan XC-72 carbon black (CB) was purchased from Cabot Corporation. All chemicals were used without further purification and all solutions used in this study were prepared by using deionized water.

2.2. Synthesis of Ni and Ni/CB catalysts

Vulcan XC-72 carbon black used as the support was first acidized with nitric acid to gain better hydrophility and better adsorptivity for metallic ions. The acidification procedure is as follows: 3.0 g of carbon black and 300 mL of concentrated nitric acid were mixed uniformly in a 500 mL round-bottom flask. The mixture was heated to 100 °C under continuously stirring and constant reflux for 12 h. The resulting carbon black was centrifuged and washed with deionized water until neutral, and then dried for further use.

Ni/CB catalysts with differing Ni content were synthesized by a facile soft chemistry method. In a typical experimental procedure for the preparation of Ni/CB catalyst with 22 wt% Ni content is as follows: 0.05 g of CB was dispersed in 70 mL of EG, followed by adding 30 mL of EG solution of $NiCl_2{\cdot}6H_2O$ (0.0122 mol L^{-1}). Then the resulting mixture was heated to 60 °C under mechanical stirring for 20 min. Finally, 8 mL of hydrazine hydrate (50%) and 5 mL of NaOH/EG (1 mol L^{-1}) solution were added into the above mixture. After 30-minute reaction, the suspension was centrifuged, washed and vacuum freeze–dried. The product was labeled as $Ni_{0.22}$/CB (the subscript represents the actual Ni loading amount determined by ICP analysis). A series of Ni/CB catalysts with differing Ni content were prepared via the same method by varying the feeding ratio and marked as $Ni_{0.002}$/CB, $Ni_{0.11}$/CB, $Ni_{0.33}$/CB, $Ni_{0.41}$/CB and $Ni_{0.49}$/CB, respectively. The above procedure was also used to synthesize pure nano Ni catalyst without CB for comparison.

2.3. Characterization

Several characterization measurements were performed on the as-prepared catalysts. The morphologies of the catalysts were characterized by transmission electron microscope (TEM, JEOL JEM-2100, 200 kV). Samples for TEM analysis were prepared by dropping the ethanol suspension of catalysts onto the 300 mesh Cu grids coated with a carbon layer. The crystal structures of as-prepared catalysts were characterized by powder X-ray diffraction (XRD) analyses using a Bruker D8 Advanced diffractometer with Cu Kα radiation (λ = 0.15406 nm), and the scanning angle ranged from 10° to 80° (2θ) at the scanning speed of 0.05 ° s^{-1}. X-ray photoelectron spectroscope (XPS) measurements were performed on a RBD-upgraded PHI-5000C ESCA system (Thermo ESCALAB 250) with Al Kα radiation ($h\nu$ = 1486.6 eV). Magnetic measurements were carried out with a vibrating sample magnetometer (VSM, Lakeshore7300) from −5000 Oe to +5000 Oe at room temperature (300 K). Inductively coupled plasma atomic emission spectrometry (ICP, Shimadzu ICPS-7510) was applied to determine the exact amounts of Ni in catalysts.

2.4. Catalytic hydrogenation reactions of nitrophenols

Catalytic hydrogenation reactions of nitrophenols in the presence of excess $NaBH_4$ were conducted in aqueous solution at atmospheric pressure and 30 °C, which can be served as the model reaction to assess the performance of Ni/CB catalysts with differing Ni content. In a typical experiment, aqueous solution of *p*-NP (0.5 mM) was freshly prepared and 5 mg of catalyst were dispersed in 10 mL of deionized water under ultrasonic radiation for several minutes until uniformly dispersed, then 2 mL of the dispersion were taken out and injected into 50 mL of *p*-NP solution under continuous stirring for 1 h to reach the adsorption-desorption equilibrium. After that, 0.1 g of $NaBH_4$ was put into the mixture with stirring. The reaction progress was evaluated by taking a small portion of the reaction mixture (diluted five times with deionized water) at specified time intervals and measuring the UV–vis spectra on PERSEE TU-1900. After the reaction, the catalyst can be easily removed from the solution phase under an external magnetic field, washed with ethanol and then reused 10 times in succession. In addition, the hydrogenation reactions of *o*-NP and *m*-NP were carried out under the same conditions. For comparison, CB and nano Ni catalyst were also participated in the hydrogenation reactions. Moreover, catalytic hydrogenation of *p*-NP was conducted at four different temperatures (20, 30, 40 and 50 °C) to evaluate the impact of the temperature on the reaction. In order to investigate the effect of sol-

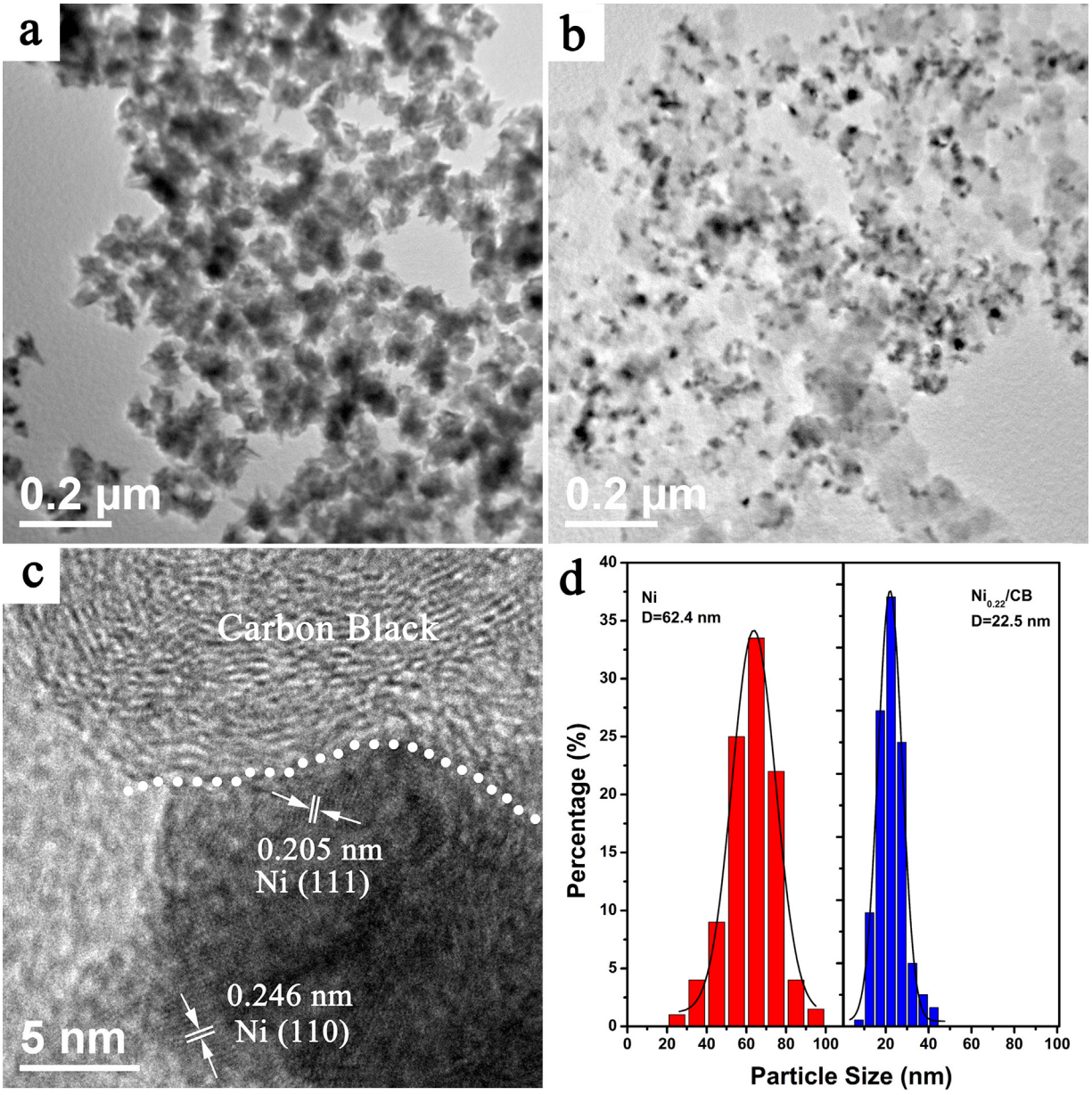

Fig. 1. (a–b) TEM images of Ni and $Ni_{0.22}$/CB catalysts; (c) High-resolution TEM image of $Ni_{0.22}$/CB catalyst; (d) Particle size distributions of nano Ni and $Ni_{0.22}$/CB catalysts.

vent on the reaction, the activity measurements were performed in methanol at 30 °C.

3. Results and discussion

3.1. Morphology and structure

The morphologies of pure Ni NPs and $Ni_{0.22}$/CB catalysts were examined by TEM, which indicate that the as-prepared pure Ni NPs have an average size of 62.4 nm (Fig. 1a and d), while in $Ni_{0.22}$/CB catalyst the Ni NPs are well dispersed on the surface of carbon black and exhibit much smaller size (22.5 nm) and much narrower size distribution (Fig. 1b and d). The lattice fringe spacing of $Ni_{0.22}$/CB was measured to be 0.205 nm and 0.246 nm, disclosing the crystal plane distances of nickel (1 1 1) and (1 1 0) planes (Fig. 1c), respectively. No obvious Ni particle aggregates can be observed due to the dispersion effect of CB.

The X-ray diffraction (XRD) patterns of Ni NPs, $Ni_{0.49}$/CB, $Ni_{0.22}$/CB and $Ni_{0.002}$/CB catalysts are shown in Fig. 2. The broad characteristic peak in the pattern of carbon black at around 24.3° is due to the (0 0 2) plane reflection of carbon materials. The intensive diffraction peaks at 44.5°, 51.8° and 76.4° are associated with the (1 1 1), (2 0 0) and (2 2 0) planes of the face-centered-cubic (fcc) structure Ni (PDF# 04-0850), respectively, suggesting a good crystallinity of the Ni NPs in the catalysts. It is necessary to note that no obvious diffraction peaks of Ni in $Ni_{0.002}$/CB can be observed because of the low Ni loading amount on the support.

As a fast and reliable technique, X-ray photoelectron spectroscopy (XPS) is widely used to analyze the chemical composition and the nature of chemical bonds. The global XPS spectrum presented in Fig. 3a shows the compositional elements of $Ni_{0.22}$/CB, indicating that carbon, oxygen and nickel are the dominant species. The Ni spectral feature of $Ni_{0.22}$/CB consists of metallic Ni as well as Ni oxide and hydroxide (Fig. 3b). In general, the Ni $2p_{3/2}$ spectrum shows a complex structure with intense satellite signals of high binding energy adjacent to the main peaks due to multi-electron excitation [43,44]. Taking account of these shake-up peaks, the peak appeared at the binding energy of 852.0 eV may be attributed to

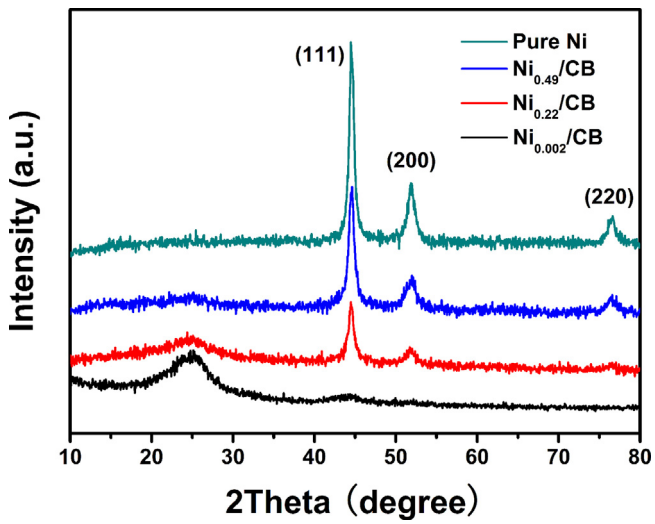

Fig. 2. XRD patterns of Ni, $Ni_{0.49}$/CB, $Ni_{0.22}$/CB and $Ni_{0.002}$/CB catalysts.

metallic Ni, the most intense doublet (855.4 eV and 873.0 eV) is due to Ni^{2+} in NiO and the second doublet (861.0 eV and 879.0 eV) can be ascribed to Ni^{2+} in $Ni(OH)_2$. The existence of NiO and $Ni(OH)_2$ is due to that the surface atoms on Ni NPs can be easily oxidized to form Ni oxide and hydroxide when exposed to air in the presence of water [45]. It should be noted that there are no peaks related to NiO or $Ni(OH)_2$ in the XRD pattern of $Ni_{0.22}$/CB (Fig. 2) and this is most likely because of the amorphous nature of resulting NiO and $Ni(OH)_2$. Moreover, the relatively weak peak of metallic Ni is due to that the XPS signals come from the surface of the sample. As shown in Fig. 3c, the C 1s spectrum can be deconvolved into five peaks with binding energies at 284.6, 285.4, 286.6, 288.2 and 290.2 eV, corresponding to various carbons under different chemical environment in the catalyst: sp^2 carbon, sp^3 carbon, C—O, C═O species and π–π^* transition loss [42].

3.2. Magnetic properties

Magnetic properties of as-prepared $Ni_{0.22}$/CB catalyst were measured by vibrating sample magnetometer at 300 K in the applied magnetic field sweeping from −5000 Oe to +5000 Oe. The typical hysteresis loop of $Ni_{0.22}$/CB in its magnetic behavior indicates the soft magnetic nature of the catalyst (Fig. 4). The saturation magnetization (*Ms*), remanent magnetization (*Mr*) and coercivity (*Hc*) values of $Ni_{0.22}$/CB catalyst are 5.19 emu g^{-1}, 1.74 emu g^{-1} and 101.6 Oe, respectively (see the left insert of Fig. 4). This suggests that $Ni_{0.22}$/CB catalyst is expected to be easily separated from the dispersion system under an external magnetic field (see the right insert of Fig. 4).

3.3. Catalytic activity for hydrogenation of nitrophenols

3.3.1. Catalytic hydrogenation of p-NP

The catalytic activity of the as-obtained catalysts was evaluated by employing the hydrogenation of *p*-NP into *p*-AP in the presence of $NaBH_4$. As shown in Fig. 5a, the yellow aqueous *p*-NP solution exhibited an absorption maximum at 317 nm. Upon the addition of $NaBH_4$, the absorption maximum at 400 nm can be attributed to the formation of 4-nitrophenolate [14,46]. In contrast, though an excessive amount of $NaBH_4$ (~100 times) was added into the *p*-NP solution, hydrogenation of *p*-NP cannot be carried out in the absence of catalyst, even for a long time of 10 h. Fig. 5b shows the UV–vis absorption spectra of reaction solution in the presence of $Ni_{0.22}$/CB catalyst at a certain time interval. It can be seen that the

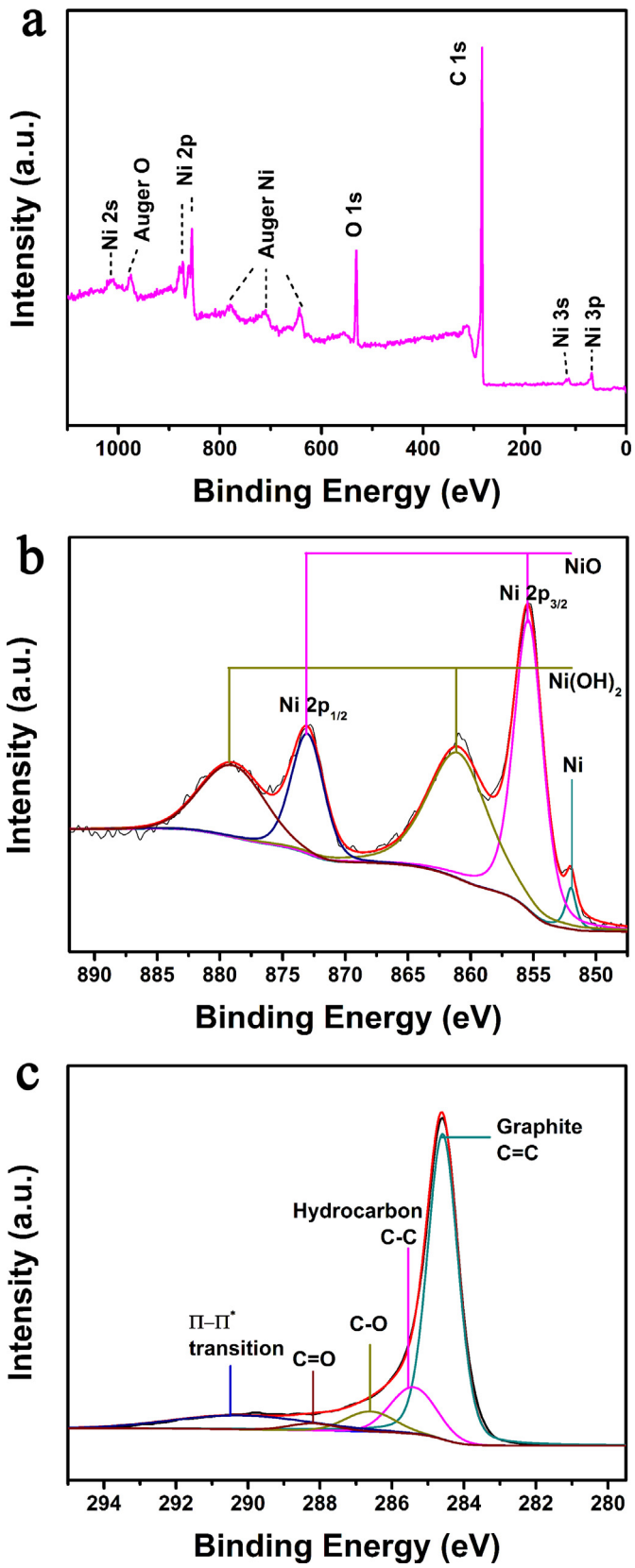

Fig. 3. (a) Global XPS spectrum of as-prepared $Ni_{0.22}$/CB catalyst; (b–c) Ni 2p and C 1s core-level XPS spectra of $Ni_{0.22}$/CB catalyst.

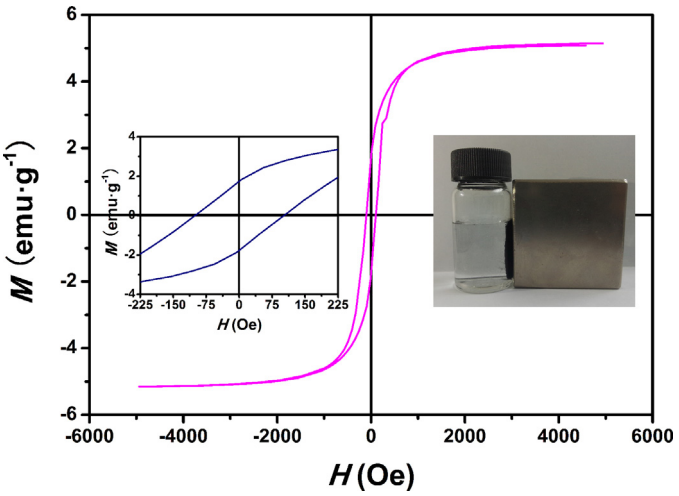

Fig. 4. Magnetic hysteresis loop of $Ni_{0.22}$/CB catalyst at the temperature of 300 K. The inserts shows the magnetic hysteresis loop in low field zone (left) and the dispersion system after magnetic separation using an external magnet (right).

intensity of the absorption peak at 400 nm corresponding to *p*-NP successively decreased as the reaction proceeded, meanwhile, a new peak with a maximum absorption at 300 nm corresponding to *p*-AP appeared and increased concomitantly with the reaction time. A plot of c/c_0 versus reaction time and pseudo-first-order plot of $\ln(c/c_0)$ against reaction time for the hydrogenation of *p*-NP over different catalysts are portrayed in Fig. 5c-d. Obviously, CB alone showed very poor catalytic activity in the reaction. It can be clearly seen from Fig. S1 the average particle size increased with the increasing Ni loading content, especially, the aggregation appeared obviously at higher loadings (Fig. S1e–f). The Ni/CB catalyst with low Ni content ($Ni_{0.002}$/CB, Fig. S1a) exhibited very low catalytic activity due to its small amount of catalytic active centers, while the catalysts with excessive Ni loadings showed an evident trend of decrease in activity with the increasing Ni loadings, which can be ascribed to the aggregation of Ni nanoparticles and relatively large particle sizes.

Taking into account the excessive amount of $NaBH_4$ (~100 times), the pseudo-first-order kinetics with respect to *p*-NP (Eq. (1)) can be used to assess the catalytic activity of the catalysts and the rate constant (k) can be calculated by a linear plot of $\ln(c/c_0)$ vs reduction time:

$$\ln \frac{c}{c_0} = -kt \quad (1)$$

$$\ln c = -kt + \ln C_0 \quad (2)$$

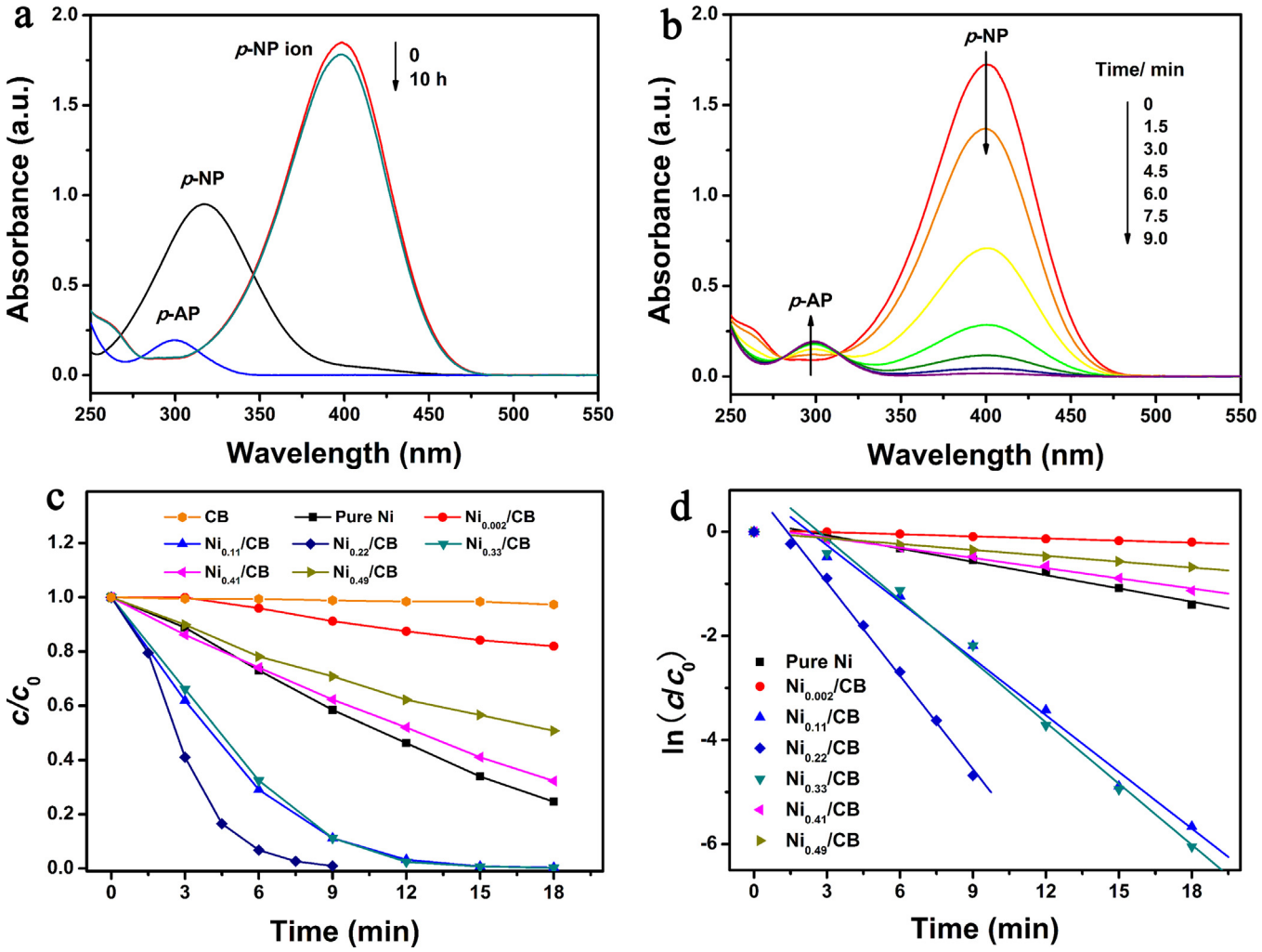

Fig. 5. (a) UV–vis absorption spectra of *p*-NP before and after adding $NaBH_4$ and its reduction product *p*-AP; (b) UV–vis absorption spectra of *p*-NP catalyzed by $Ni_{0.22}$/CB catalyst at a certain time interval; (c) c/c_0 versus time for the hydrogenation of *p*-NP over different catalysts; (d) Pseudo-first-order plot of $\ln(c/c_0)$ against reaction time for the hydrogenation of *p*-NP over different catalysts.

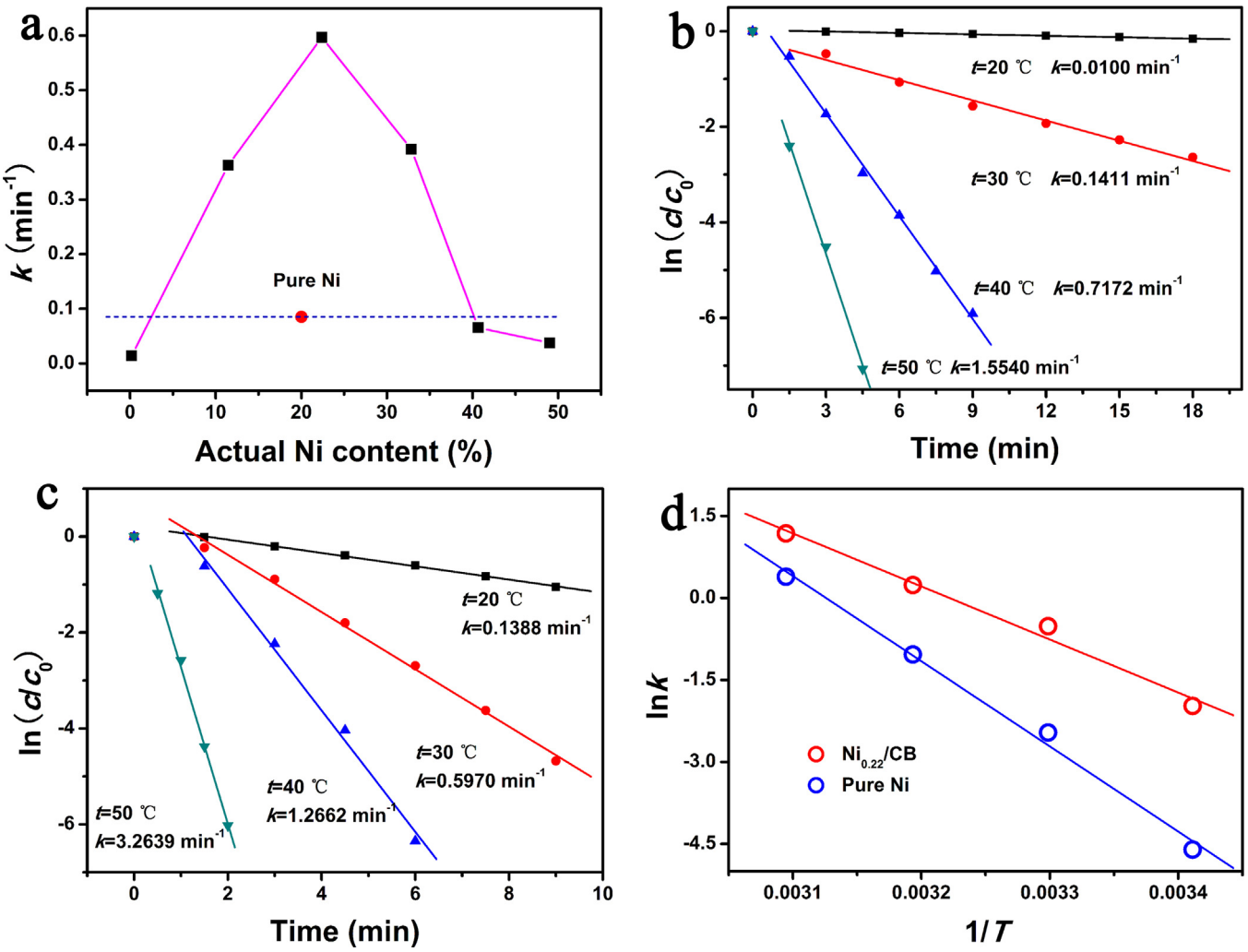

Fig. 6. (a) The relationship between kinetic constant and actual Ni content; (b–c) Pseudo-first-order plot of $\ln(c/c_0)$ against reaction time for the hydrogenation of *p*-NP catalyzed by Ni and $Ni_{0.22}$/CB catalysts at different temperatures; (d) Plot of ln*k* against 1/*T* for the catalytic reduction of *p*-NP.

Table 1
Pseudo-first-order kinetics study of *p*-NP reduction over different catalysts at 30 °C [a].

Entry	Catalyst	k/ (min^{-1})	R^2
1	$Ni_{0.002}/CB$	0.0136	0.9921
2	$Ni_{0.11}/CB$	0.3628	0.9900
3	$Ni_{0.22}/CB$	0.5970	0.9959
4	$Ni_{0.33}/CB$	0.3921	0.9910
5	$Ni_{0.41}/CB$	0.0653	0.9912
6	$Ni_{0.49}/CB$	0.0376	0.9970
7	Ni	0.0852	0.9898

[a] p-Nitrophenol (0.5 mmol L^{-1}, 50 mL), catalyst suspension (0.5 mg mL^{-1}, 2 mL), $NaBH_4$ (0.1 g), 30 °C.

where *c* is the concentration of *p*-NP that changes during the time, c_0 is the initial concentration of *p*-NP, *k* is the rate constant and *t* is the reaction time. The calculated kinetic rate constants are listed in Table 1, where we can find that *k* (0.5970 min^{-1}) of $Ni_{0.22}$/CB is impressively higher than that of recently reported nickel-based nanocatalysts [1,2,18].

3.3.2. Effect of temperature on the reduction of p-NP and activation energy for reaction

As shown in Fig. 6a, catalytic hydrogenation of *p*-NP over $Ni_{0.22}$/CB exhibits the highest reaction rate constant among the catalysts with differing Ni content. $Ni_{0.22}$/CB and unsupported Ni catalyst were chosen as the samples to evaluate the effect of temperature on the reduction of *p*-NP since the reaction temperature is one of essential factors for the reduction of *p*-NP. The catalytic hydrogenation of *p*-NP over $Ni_{0.22}$/CB and unsupported Ni catalyst were carried out at four different temperatures ranging from 20 °C to 50 °C with an excessive amount of $NaBH_4$ (~100 times) under ambient pressure. As shown in Fig. 6b and c, the rate constant *k* increases with the rise of temperature. According to the Arrhenius equation (Eq. (3)) and the linear relationship of ln*k* against 1/*T* (Eq. (4), Fig. 6d), the apparent activation energies (E_a) of the catalytic hydrogenation of *p*-NP over $Ni_{0.22}$/CB and unsupported Ni catalyst are calculated to be 80.75 kJ mol^{-1} and 129.31 kJ mol^{-1}, respectively, indicating that combination of Ni nanoparticles and carbon black greatly reduces the activation energy, which facilitates the reaction at lower temperatures and energy saving.

$$k = Ae^{-\frac{E_a}{RT}} \quad (3)$$

$$\ln k = \left(-\frac{E_a}{R}\right)\frac{1}{T} + \ln A \quad (4)$$

3.3.3. Cycling performance

To explore hydrogenation catalysts with high activity coupled with convenient recoverability and stable reusability is of great importance. The $Ni_{0.22}$/CB and unsupported Ni catalysts were used in the reduction reaction of *p*-NP for 20 min at 30 °C over 10 cycles. As shown in Fig. 7, cycling performance of either $Ni_{0.22}$/CB or unsup-

Table 2
Substituent effects on the catalytic hydrogenation of nitrophenols[a].

Entry	Catalyst	Solvent	Product	Reaction time (min)	Conversion(%)	Reaction time (min)	Conversion(%)
1			*o*-AP	5	54.4	15	100
2	$Ni_{0.22}$/CB	H_2O	*m*-AP	5	87.6	15	100
3			*p*-AP	5	87.0	15	100
4			*o*-AP	3	85.7	5	100
5	$Ni_{0.22}$/CB	MeOH	*m*-AP	3	100	5	100
6			*p*-AP	3	100	5	100
7			*o*-AP	5	46.1	15	85.7
8	Ni	H_2O	*m*-AP	5	54.5	15	100
9			*p*-AP	5	58.6	15	89.7

[a] p-Nitrophenol (0.5 mmol L^{-1}, 50 mL), catalyst suspension (0.5 mg mL^{-1}, 2 mL), $NaBH_4$ (0.1 g), 30 °C.

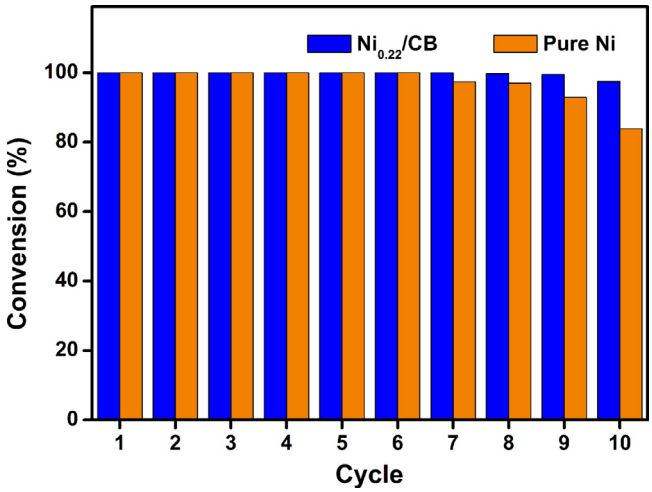

Fig. 7. Cycling performance of Ni and $Ni_{0.22}$/CB catalysts for *p*-NP reduction.

ported Ni catalyst can be recycled for 6 successive cycles of reaction without noticeable decay in activity. Even after 10 cycles, the conversion of *p*-NP over $Ni_{0.22}$/CB still maintained over 95 %, while for unsupported Ni catalyst, only 83 % conversion can be reached, suggesting the excellent stability of $Ni_{0.22}$/CB for the catalytic reaction.

3.3.4. Substituent effects on the catalytic hydrogenation of nitrophenols

Catalytic hydrogenation of *o*-NP and *m*-NP was also carried out with an excessive amount of $NaBH_4$ in the presence of $Ni_{0.22}$/CB and the unsupported Ni catalyst. As listed in Table 2, *m*-NP shows the highest reactivity in aqueous or methanol system and completed conversion into *m*-AP can be achieved within 15 min. While *o*-NP exhibits the lowest reactivity. The difference in reactivity of individual nitrophenols may be explained in terms of the conjugation effect, inductive effect, steric effect and/or molecular orientation of the substituent group [1]. It is known that *o*-NP and *p*-NP may be stabilized to some extent by the conjugation effect which delocalizes the negative charge in the phenoxide ion into the nitro group. Furthermore, taking into account of the inductive effect, the distance between -OH and $-NO_2$ in *o*-NP is shorter than that in *p*-NP. Thereby, stronger inductive effect leads to more positively charged nitrogen atom in *o*-NP. Hydrogenation reaction of nitrophenols starts from the attack by negatively charged active hydrogen against the nitrogen atom, so *o*-NP with more positively charged nitrogen atom would be expected to have high reactivity [9]. However, *o*-NP exhibited the lowest reactivity, suggesting that the steric effect play a predominant role among the various effects. In the case of *m*-NP, there is no direct conjugation effect between the meta-nitro group and the phenoxide oxygen, stabilization of the nitro group by the inductive effect alone is limited. Consequently, the nitro group of *m*-NP shows higher reactivity than that of *p*-NP or *o*-NP. Moreover, it is interesting that all the nitrophenols exhibit higher reactivity in methanol than that in aqueous solution (Table 2). This phenomenon is related to the concentration of hydrogen in the reaction system. Fig. S2 shows that at a given time, the methanol-$NaBH_4$ reaction system yielded much more amount of hydrogen than the water-$NaBH_4$ system, which may explain why the reaction occurs more quickly in methanol than in water.

3.3.5. Mechanistic insight into the reaction of nitrophenols hydrogenation

Based on the experimental results and the literatures [3,9,21,24], it can be understood that the present reduction process involves the following crucial steps as shown in Scheme 1: (1) In the

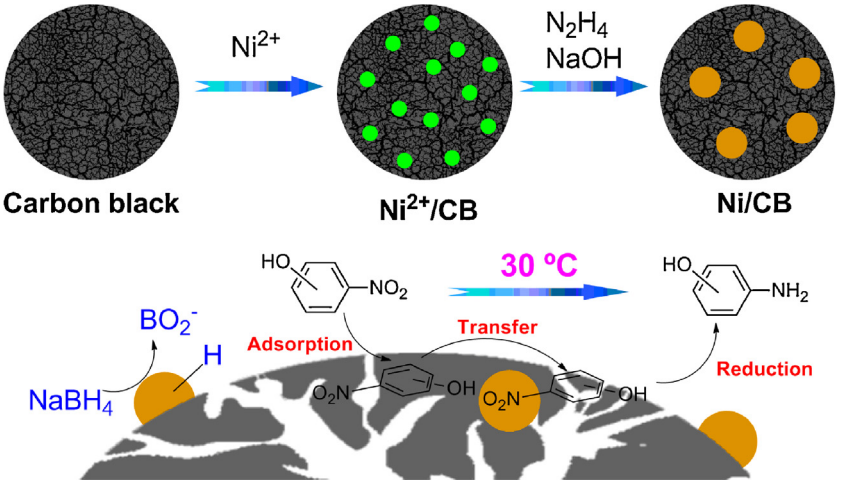

Scheme 1. Possible mechanisms of catalyst preparation and catalytic hydrogenation of nitrophenols.

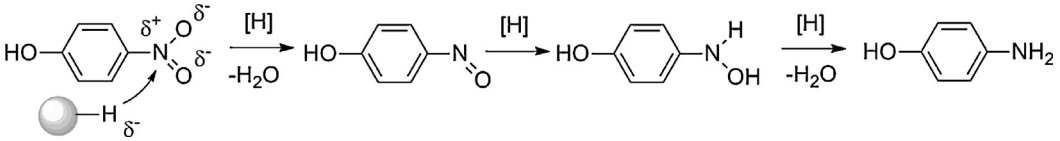

Scheme 2. Hydrogenation process of p-NP with several intermediate products by using $Ni_{0.22}$/CB catalyst.

reaction system, the π-π stacking interaction between aromatic nitrophenol molecules and the surface of CB plays an important role in promoting the aromatic entities gaining easier access to Ni NPs. Nitro group with strong electro-withdrawing ability could enhance the π-π stacking interaction between CB and nitrophenols [47,48]. (2) $NaBH_4$ reacts with water at room temperature to slowly produce H_2 and sodium metaborate ($NaBO_2$). With the presence of Ni NPs, the H—H bond of the adsorbed H_2 cleaves followed by the formation of nickel-hydrogen bonds. (3) The positively charged nitrogen in the nitro group of nitrophenols can be readily attacked by hydrogen with a partial negative charge due to the electronegativity discrepancy between hydrogen and metallic atoms. The nitro group is first reduced to the nitroso group, and then turns into hydroxylamine by the reductive addition of two hydrogen atoms, which is further reduced to the aminophenol (Scheme 2). The high activity of $Ni_{0.22}$/CB observed here can be attributed to the specific characteristics of the nanostructure of the catalyst and the synergistic effect of Ni NPs and carbon black. First of all, the porous carbon black has high specific surface area and plenty of oxygen-containing groups (Fig. S3) for anchoring Ni atoms, which is in favor to disperse and stabilize the catalytic system. Secondly, carbon black has strong adsorption ability for organic molecules, which provides a higher concentration of *p*-NP near to the Ni NPs on carbon black, leading to highly efficient contact between the reactant molecules and the active sites [37,49]. Thirdly, since carbon black is a conductive matrix, electron transfer from the carbon black to Ni nanoparticles increases the local electron density, facilitating the uptake of electrons by *p*-NP molecules.

4. Conclusions

In summary, a nano-Ni/carbon black catalyst was successfully prepared by a facile soft chemistry method. The as-obtained catalyst exhibits high performance for hydrogenation of nitrophenols to aminophenols at 30 °C, which is significantly superior to those reported recently by others on nickel-based nanocatalysts [1,2,18]. The high catalytic activity of the catalyst can be ascribed to the specific characteristics of the nanostructure of the catalyst and the synergistic effect of Ni NPs and carbon black. Moreover, the Ni/CB catalyst is not only cheap but also magnetically separable, and therefore, this approach facilitates achieving the cost-effective reduction of nitrophenols to aminophenols.

Acknowledgements

This work was supported by NNSF of China (Nos. 51322212), RFDP (No.20123219130003), the Fundamental Research Funds for the Central Universities (No. 30920140122008), and PAPD of Jiangsu.

Appendix A. Supplementary data

Supplementary data associated with this article can be found, in the online version, at http://dx.doi.org/10.1016/j.apcatb.2015.06.043

References

[1] N. Sahiner, H. Ozay, O. Ozay, N. Aktas, Appl. Catal. A 385 (2010) 201–207.
[2] Z. Jiang, J. Xie, D. Jiang, X. Wei, M. Chen, CrystEngComm 15 (2013) 560–569.
[3] Y. Wu, M. Wen, Q. Wu, H. Fang, J. Phys. Chem. C 118 (2014) 6307–6313.
[4] N. Sahiner, S. Yildiz, H. Al-Lohedan, Appl. Catal. B 166 (2015) 145–154.
[5] J. Feng, L. Su, Y. Ma, C. Ren, Q. Guo, X. Chen, Chem. Eng. J. 221 (2013) 16–24.
[6] D. Sreekanth, D. Sivaramakrishna, V. Himabindu, Y. Anjaneyulu, J. Hazard. Mater. 164 (2009) 1532–1539.
[7] Z. Dong, X. Le, C. Dong, W. Zhang, X. Li, J. Ma, Appl. Catal. B 162 (2015) 372–380.
[8] M.K.K. Oo, C. Chang, Y. Sun, X. Fan, Analyst 136 (2011) 2811–2817.
[9] J. Sun, Y. Fu, G. He, X. Sun, X. Wang, Catal. Sci. Technol. 4 (2014) 1742–1748.
[10] M.A. Harrison, S. Barra, D. Borghesi, D. Vione, C. Arsene, R. Iulian Olariu, Atmos. Environ. 39 (2005) 231–248.
[11] C. Yeh, D. Chen, Appl. Catal. B 150 (2014) 298–304.
[12] J. Chiou, B. Lai, K. Hsu, D. Chen, J. Hazard. Mater. 248 (2013) 394–400.
[13] Z. Wu, J. Chen, Q. Di, M. Zhang, Catal. Commun. 18 (2012) 55–59.
[14] I.H. Abd El Maksod, E. Hegazy, S. Kenawy, T. Saleh, Appl. Surf. Sci. 255 (2009) 3471–3479.
[15] J. Ding, L. Chen, R. Shao, J. Wu, W. Dong, React. Kinet. Mech. Catal. 106 (2012) 225–232.
[16] I.H. Abd El Maksod, T.S. Saleh, Green Chem. Lett. Rev. 3 (2010) 127–134.
[17] H. Liu, J. Deng, W. Li, Catal. Lett. 137 (2010) 261–266.
[18] Z. Ji, X. Shen, G. Zhu, H. Zhou, A. Yuan, J. Mater. Chem. 22 (2012) 3471–3477.
[19] S. Zhang, S. Gai, F. He, S. Ding, L. Li, P. Yang, Nanoscale 6 (2014) 11181–11188.
[20] Y. Shen, Y. Sun, L. Zhou, Y. Li, E.S. Yeung, J. Mater. Chem.A 2 (2014) 2977–2984.
[21] C. Wen, A. Yin, W. Dai, Appl. Catal. B 160 (2014) 730–741.
[22] Y. Yang, C. Sun, X. Li, F. Yang, W. Zhang, X. Zhang, Y. Ren, Appl. Catal B 165 (2015) 94–102.
[23] A. Wang, H. Yin, H. Lu, J. Xue, M. Ren, T. Jiang, Langmuir 25 (2009) 12736–12741.
[24] X. Li, K. Wu, Y. Ye, X. Wei, Nanoscale 5 (2013) 3648–3653.
[25] J.A. Johnson, J.J. Makis, K.A. Marvin, S.E. Rodenbusch, K.J. Stevenson, J. Phys. Chem. C 117 (2013) 22644–22651.
[26] S. Rana, K. Parida, Catal. Sci. Technol. 2 (2012) 979–986.
[27] M. Crespo-Quesada, A. Yarulin, M. Jin, Y. Xia, L. Kiwi-Minsker, J. Am. Chem. Soc. 133 (2011) 12787–12794.
[28] S. Pandey, S.B. Mishra, Carbohydr. Polym. 113 (2014) 525–531.
[29] M. Goepel, M. Al-Naji, P. With, G. Wagner, O. Oeckler, D. Enke, R. Gläser, Chem. Eng. Technol. 37 (2014) 551–554.
[30] H. Ma, H. Wang, C. Na, Appl. Catal. B 163 (2015) 198–204.
[31] P. Etayo, A. Vidal-Ferran, Chem. Soc. Rev. 42 (2013) 728–754.
[32] R.R. Dykeman, N. Yan, R. Scopelliti, P.J. Dyson, Inorg. Chem. 50 (2011) 717–719.
[33] M.J. Hanton, S. Tin, B.J. Boardman, P. Miller, J. Mol. Catal. A: Chem. 346 (2011) 70–78.
[34] S. Wesselbaum, T. vom Stein, J. Klankermayer, W. Leitner, Angew. Chem. 124 (2012) 7617–7620.
[35] E. Seo, J. Kim, Y. Hong, Y.S. Kim, D. Lee, B.-S. Kim, J. Phys. Chem. C 117 (2013) 11686–11693.
[36] C. Lin, K. Tao, D. Hua, Z. Ma, S. Zhou, Molecules 18 (2013) 12609–12620.
[37] T. Ji, L. Li, M. Wang, Z. Yang, X. Lu, RSC Adv. 4 (2014) 29591–29594.
[38] S. ur Rehman, M. Siddiq, H. Al-Lohedan, N. Sahiner, Chem. Eng. J. 265 (2015) 201–209.
[39] A. Wang, H. Yin, M. Ren, H. Lu, J. Xue, T. Jiang, New J. Chem. 34 (2010) 708–713.
[40] M. Ajmal, M. Siddiq, H. Al-Lohedan, N. Sahiner, RSC Adv. 4 (2014) 59562–59570.
[41] S. Gowda, D. Gowda, Tetrahedron 58 (2002) 2211–2213.
[42] H. Estrade-Szwarckopf, Carbon 42 (2004) 1713–1721.
[43] K. Park, J. Choi, B. Kwon, S. Lee, Y.-E. Sung, H. Ha, S.-A. Hong, H. Kim, A. Wieckowski, J. Phys. Chem. B 106 (2002) 1869–1877.
[44] S. Shen, T. Zhao, J. Xu, Y. Li, J. Power Sources 195 (2010) 1001–1006.
[45] W. Lin, H. Cheng, J. Ming, Y. Yu, F. Zhao, J. Catal. 291 (2012) 149–154.
[46] N. Pradhan, A. Pal, T. Pal, Langmuir 17 (2001) 1800–1802.
[47] Q. Liu, T. Zheng, P. Wang, J. Jiang, N. Li, Chem. Eng. J. 157 (2010) 348–356.
[48] F. Cozzi, M. Cinquini, R. Annuziata, J.S. Siegel, J. Am. Chem. Soc. 115 (1993) 5330–5331.
[49] T.J. Bandosz, C. Petit, J. Colloid Interface Sci. 338 (2009) 329–345.